Research Square

Preprints are preliminary reports that have not undergone peer review.
They should not be considered conclusive, used to inform clinical practice,
or referenced by the media as validated information.

A dry lunar mantle reservoir for young mare basalts of Chang'E-5

Sen Hu (husen@mail.iggcas.ac.cn)
Institute of Geology and Geophysics, Chinese Academy of Sciences

Huicun He
Institute of Geology and Geophysics, Chinese Academy of Sciences

Jianglong Ji
Institute of Geology and Geophysics, Chinese Academy of Sciences

Yangting Lin
Institute of Geology and Geophysics

Hejiu Hui
Nanjing University https://orcid.org/0000-0003-2707-4977

Mahesh Anand
The Open University https://orcid.org/0000-0003-4026-4476

Romain Tartese
The University of Manchester https://orcid.org/0000-0002-3490-9875

Yihong Yan
Institute of Geology and Geophysics, Chinese Academy of Sciences

Jialong Hao
Institute of Geology and Geophysics

Ruiying Li
Institute of Geology and Geophysics, Chinese Academy of Sciences

Lixin Gu
Institute of Geology and Geophysics, Chinese Academy of Sciences

Qian Guo
Institute of Geology and Geophysics, Chinese Academy of Sciences

Huaiyu He
Chinese Academy of Sciences

Zi-Yuan Ouyang
National Astronomical Observatories, Chinese Academy of Sciences

Physical Sciences - Article

Keywords: young mare basalt samples, lunar water, lunar mantle reservoir, Chang'E-5

Posted Date: August 9th, 2021

DOI: https://doi.org/10.21203/rs.3.rs-764407/v1

License: This work is licensed under a Creative Commons Attribution 4.0 International License.
Read Full License

Version of Record: A version of this preprint was published at Nature on October 19th, 2021. See the published version at https://doi.org/10.1038/s41586-021-04107-9.

A dry lunar mantle reservoir for young mare basalts of Chang'E-5

Sen Hu[1]*, Huicun He[1], Jianglong Ji[1], Yangting Lin[1]*, Hejiu Hui[2], Mahesh Anand[3,4], Romain Tartèse[5], Yihong Yan[1], Jialong Hao[1], Ruiying Li[1], Lixin Gu[1], Qian Guo[6] Huaiyu He[6] & Ziyuan Ouyang[7]

[1]Key Laboratory of the Earth and Planetary Physics, Chinese Academy of Sciences, Beijing, 100029, China
[2]State Key Laboratory for Mineral Deposits Research& Lunar and Planetary Science Institute, School of the Earth Sciences and Engineering, Nanjing University, Nanjing, Jiangsu 210023, China
[3]School of Physical Sciences, The Open University, Milton Keynes, MK7 6AA, UK
[4]Department of Earth Sciences, The Natural History Museum, London, SW7 5BD, UK
[5]Department of Earth and Environmental Sciences, The University of Manchester, Manchester, M13 9PL, UK
[6]State Key Laboratory of Lithospheric Evolution, Chinese Academy of Sciences, Beijing, 100029, China
[7]Center for lunar and planetary sciences, Institute of Geochemistry, Chinese Academy of Sciences, Guiyang, 550081, China
*Correspondence to: husen@mail.iggcas.ac.cn, linyt@mail.iggcas.ac.cn, 19 Beituchengxi Road, Chaoyang District, Beijing, 100029, China

The distribution of water in the Moon's interior carries key implications for the origin of the Moon[1], the crystallisation of the lunar magma ocean[2], and the duration of lunar volcanism[2]. The Chang'E-5 (CE5) mission returned the youngest mare basalt samples, dated at ca. 2.0 billion years ago[3], from the northwestern Procellarum KREEP Terrane (PKT), providing a probe into the spatio-temporal evolution of lunar water. Here we report the water abundance and hydrogen isotope composition of apatite and ilmenite-hosted melt inclusions from CE5 basalts, from which we derived a maximum water abundance of 370 ± 30 μg.g^{-1} and a δD value (-330 ± 160‰) for their parent magma. During eruption, hydrogen degassing led to an increase in the D/H ratio of the residual melts up to δD values of 300-900‰. Accounting for low degrees of mantle partial melting followed by extensive magma fractional crystallisation[4], we estimate a maximum mantle water abundance of 2-6 μg.g^{-1}, which are too low for water contents alone to account for generating the Moon's youngest basalts. Such modest water abundances for the lunar mantle are at the lower end of those estimated from mare basalts that erupted from ca. 4.0-2.8 Ga[5, 6], suggesting the mantle source of CE5 basalts dried up by ca. 2.0 Ga through previous melt extraction from the PKT mantle during prolonged volcanic activity.

Water abundance in the lunar mantle places strict constraints on high-temperature processes, including the Moon-forming giant impact[1], the ensuing crystallisation of the lunar magma ocean[7], and the longevity of volcanism on the Moon[2]. Based upon the analyses carried out since the Apollo era, the Moon was long thought to be an anhydrous body. Advances in *in situ* analytical techniques over the past decade have allowed analysis of water abundances at micro-scale in various lunar samples, including in olivine- and pyroxene-hosted melt inclusions in mare basalts [8-12], apatite in mare basalts and highlands samples[13-20], pyroclastic glass beads[21, 22], and

anorthosites[23, 24]. The estimates of water abundances for their mantle source regions span a wide range from ~0.3 to 200 μg.g^{-1} [25], suggesting that the Moon's interior is not as anhydrous as previously thought. However, many questions remain regarding the origin(s) and distribution of water in the Moon's interior[25, 26]. The large variation in the estimated water abundances may be indicative of geographical and/or temporal heterogeneity in water abundance as these samples were collected from different regions and crystallised between ca. 4.0 to 2.8 Ga[5, 6]. Hence, additional sample collections of younger basalts from new regions can have critical implications to investigate the spatiotemporal evolution of water in the Moon. This large range of estimates could also be affected by the mixing of endogenous water with various exogenic water sources, i.e. asteroids, comets, and solar wind[19, 26, 27], and/or by interplay between many processes, such as volatile degassing, partial melting, fractional crystallisation, impacting, mixing with potassium (K), rare earth elements (REE) and phosphorus (P) (KREEP)-rich components, and spallation[11, 15, 25, 27-29]. It is thus crucial to combine *in situ* analysis of water abundances and hydrogen isotope composition with detailed contextual petrographic information.

The Chang'E-5 (CE5) mission successfully returned 1.731 kg of lunar soil samples from young mare basalt units dated at ca. 1.2-2.0 Ga using crater counting chronology[30, 31]. These returned samples have now been precisely dated at 2030 ± 4 million years ago (Ma) using the Pb-Pb isotope isochron technique[3]. The CE5 basalts are thus much younger than the youngest lunar basalt dated so far (ca. 2.8 Ga[5]). The young basalt unit is located in northwestern Oceanus Procellarum, on the northwestern edge of the Procellarum KREEP Terrane (PKT), which is far from all landing sites of the Apollo and Luna missions (Extended Data Fig. 1). The PKT region is also thought to have enhanced concentrations of two major radioactive heat-producing elements, uranium (U) and thorium (Th), and other incompatible elements. Water behaves as a typical incompatible element during magmatic processes and thus is expected to be enriched in the PKT as well. Hence, the CE5 basalts provide a unique opportunity to constrain the water inventory of a newly sampled region of the Moon's interior, providing crucial information to account for the prolonged activity of lunar magmatism.

We studied a total of 23 basalt clasts (0.2-1.5 mm in size) from two of the CE5 soil samples (CE5C0100YJFM00103, ~1g, CE5C0400YJFM00406, ~2g) (Extended Data Table 1). These basalt clasts exhibit variable textures including subophitic, poikilitic, and equigranular, similar to those observed for other basalt clasts in CE5 soil sample[3, 4], and are mainly composed of pyroxene and plagioclase with less abundant olivine and ilmenite (Figs. 1, S1 and S2). These basalt clasts are likely representative of various locations in the same lava flow, based on their identical mineral chemistry and geochemistry[4] and their well-defined Pb-Pb isochron[3]. The textures of ilmenite in the clasts indicate that it crystallised early from the melt and continued until the last stages of melt evolution (Fig. S1). Ilmenite-hosted melt inclusions range in size of ~4-50 μm in diameter and display post-entrapment crystallisation textures (~0-40%) (Figs. 1 and S1). Apatite is the main OH-bearing phase, and is F-rich than Cl-poor, similar to those from Apollo mare basalts (Fig. S6). It is an accessory phase, comprising less than 0.4 vol% modal abundance in the CE5 basalt clasts (Table S1). The apatite occurs as euhedral grains (mostly <10 μm) mainly in the fine-grained interstitial materials, with a few euhedral crystals enclosed in the margins of pyroxene (Fig. 1) and FeO-rich olivine (Fig S2, details see Supporting Information). Eight ilmenite-hosted melt inclusions and several apatite grains were located and identified from the studied CE5 basalt clasts (Extended Data Table 1 and Figs. 1, S1 and S2), and selected for *in*

situ analysis. The water abundance and hydrogen isotope compositions of ilmenite-hosted melt inclusions, apatite, and clinopyroxene from these CE5 basalt clasts were measured using a Nano-scale Secondary Ion Mass Spectrometer (NanoSIMS 50L) instrument (see Methods).

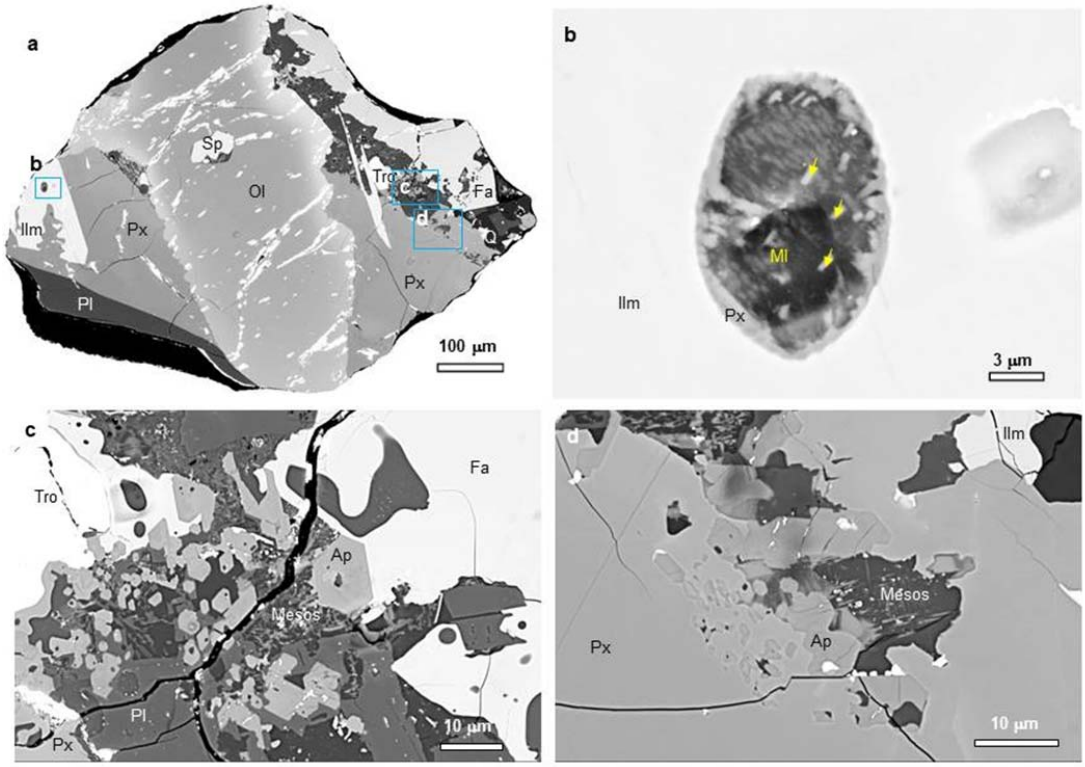

Fig. 1 | Backscattered electron (BSE) images of ilmenite-hosted melt inclusions and apatite from a CE5 basalt clast. **a**, The basalt clast (406-010,023) embedded in the metal mount is mainly composed of olivine (Ol), pyroxene (Px), plagioclase (Pl), and ilmenite (Ilm), with minor fayalite (Fa), troilite (Tro), spinel (Sp), apatite (Ap), and silica (Q). **b**, High resolution BSE image of a melt inclusion hosted in ilmenite. This melt inclusion displays a post-entrapment crystallisation texture with occurrences of submicron-sized pyroxene and merrillite (yellow arrows). **c**, High resolution BSE image of apatite in the interstitial areas. Many euhedral apatite grains, up to 10 μm in length, coexist with fine-grained plagioclase, fayalite, and mesostasis (Mesos). **d**, Small apatite grains also occur at the rims of pyroxene, coexisting with mesostasis. The bright pits in cracks are the remains of Au coating.

The majority of apatite grains contain water abundances of 555 ± 31 μg.g^{-1} to 4856 ± 217 μg.g^{-1} (avg. 1921 ± 910 μg.g^{-1}, 1σ) with δD values ranging from 275 ± 69‰ to 1022 ± 71‰ (avg. 578 ± 208‰, 1σ) (δD = 1000 × ([D/H$_{sample}$]/[D/H$_{standard}$]-1), using Vienna standard mean ocean water as the standard) (Fig. 2 and Extended Data Table 2), which overlap with apatite water abundances and δD values measured in Apollo high-Ti and low-Ti basalts[11, 15-17, 28, 29, 32-35]. Three apatite analyses yielded lower water abundances (110 ± 13 μg.g^{-1} to 235 ± 19 μg.g^{-1}; Extended Data Table 2), with corresponding δD values indistinguishable from the majority of other analyses. Because apatite is the major water-bearing phase in CE5 basalts, a water abundance of ~8 ± 4 μg.g^{-1} for the bulk CE5 basalts was calculated from the average water content of apatite

and its modal abundance of 0.4 vol% (See Supporting Information). It should be noted that this water abundance is not the original water abundance in the CE5 basalts' parent magma before eruption, but represents the residual water abundance after magma degassing at the time of apatite crystallisation[14]. Furthermore, the apatite δD values reflect the signature of the last residual melt after precipitation of most constituent minerals, and the observed large D-enrichment is likely the result of degassing of H-bearing species from the melt, mostly in the form of H_2 under the reducing conditions at the Moon[15].

The ilmenite-hosted melt inclusions contain lower water abundances of 13 ± 4 $\mu g.g^{-1}$ to 661 ± 37 $\mu g.g^{-1}$, with δD values ranging from -332 ± 182‰ to 869 ± 224‰ after correcting for the effects of cosmic ray spallation (Fig. 3 and Extended Data Table 3). Cosmic ray spallation mainly produces deuterium, and can have a large effect on δD values especially for the water-poor melt inclusions (<30 $\mu g.g^{-1}$)[36]. The cosmic ray exposure (CRE) ages determined for various Apollo lunar samples are mostly younger than ca. 200 Ma[37], but have not yet been measured for CE5 samples. We have modeled the spallation effects on δD values of the melt inclusions, using CRE ages of 10, 50, 100 and 200 Ma (see Methods and Extended Data Fig. 3). Using CRE ages from 100 to 200 Ma, the δD values yield noticeable over-correction as the resulting values are even more D-depleted than the presently accepted hydrogen isotope composition of the lunar mantle (Extended Data Fig. 4). On the Moon, Apollo regolith from a depth of ~9 mm is thought to overturn at least once in approximately 10 million years[38], suggesting that it is reasonable to assume a CRE age of ca. 50 Ma for the CE5 basalt clasts. With a 50 Ma CRE age correction, the melt inclusions with the lowest H_2O abundances yield corrected δD values of 200 ± 300‰ that overlap with the lowest δD value measured for apatite. Importantly, this correction does not greatly affect the δD values of water-rich melt inclusions nor those of apatite grains (Extended Data Fig. 4 and Tables 2 and 3). Moreover, spallation by cosmic rays has little effect on water abundances. After correction for spallation, the melt inclusions with δD ≤ 200 ‰ display a negative correlation between water abundances (13 ± 4 $\mu g.g^{-1}$ to 367 ± 29 $\mu g.g^{-1}$) and δD values (-332 ± 182‰ to 202 ± 390‰), except for three analyses with higher δD values (271 ± 113‰ to 869 ± 224‰) that overlap with the data for the water-poor apatite grains (Fig. 2 and Extended Data Table 3). These observations provide convincing evidence that ilmenite-hosted melt inclusions recorded the progressive evolution of melts undergoing degassing of H_2, resulting in considerable D-enrichment during crystallisation of the CE5 basalts[15, 39]. Diffusion out of the melt inclusions is another process by D/H ratios can be fractionated as reported for melt inclusions enclosed in olivine and pyroxene from Apollo basalts[11]. At present there is no constraints on diffusion rate of water in ilmenite-hosted melt inclusions. The lowest δD value of ~-300 ‰ measured in ilmenite-hosted melt inclusions suggests little exchange of hydrogen isotopes with the D-enriched residual melt through diffusion.

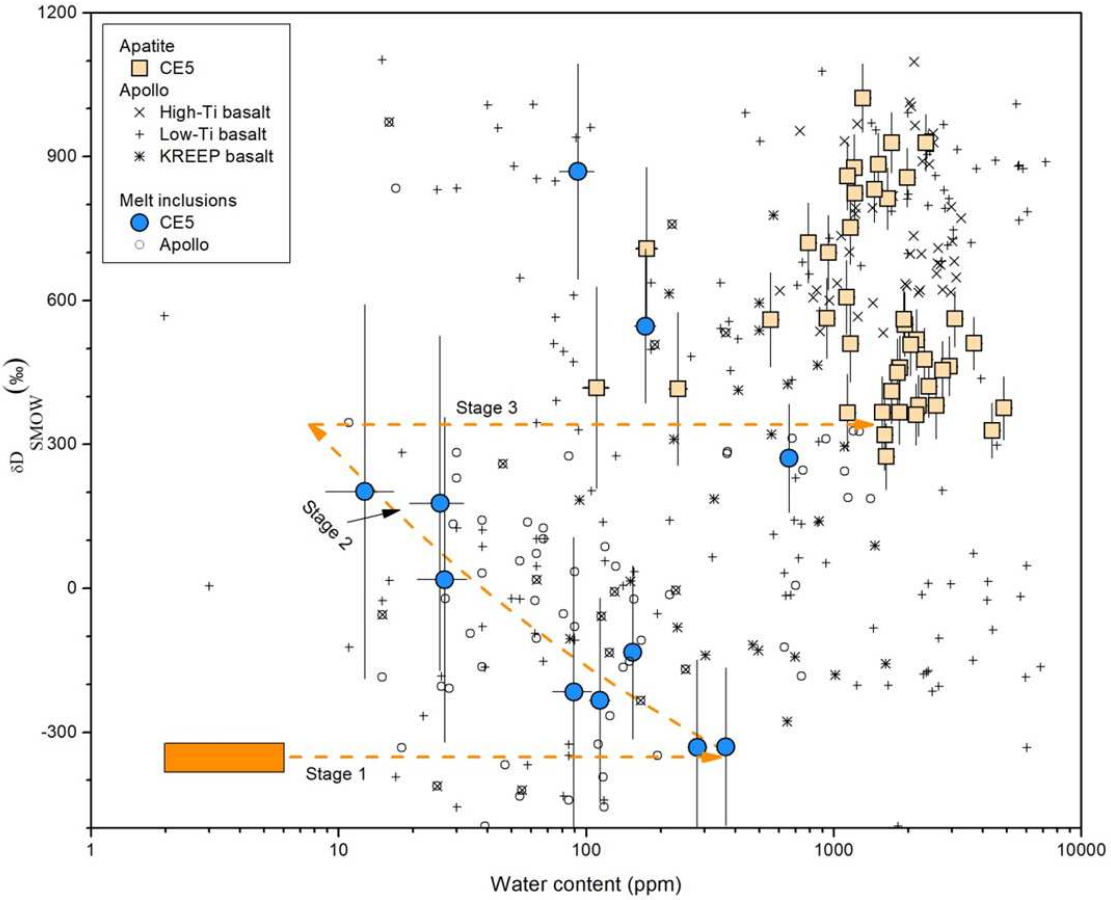

Fig. 2 | Water abundance and δD of apatite and ilmenite-hosted melt inclusions from CE5 basalts. The majority of melt inclusions display a negative correlation between the water abundance and δD values, except for a few melt inclusions with higher δD values plotting close to the range of apatite. The dotted lines indicate a three-stage evolutionary path, starting with ~2-3% partial melting of the mantle source of CE5 basalts, followed by ~43-78% fractional crystallisation (Stage 1), H_2 degassing from the basaltic melts accompanied with D-enrichment (Stage 2), and crystallisation of apatite from the residual melts, possibly accompanied by further H_2 degassing (Stage 3). Apatite and melt inclusion data from Apollo samples (Table S5) are shown for comparison. The CE5 data have been corrected for a nominal cosmic-ray exposure of 50 Ma (see Methods).

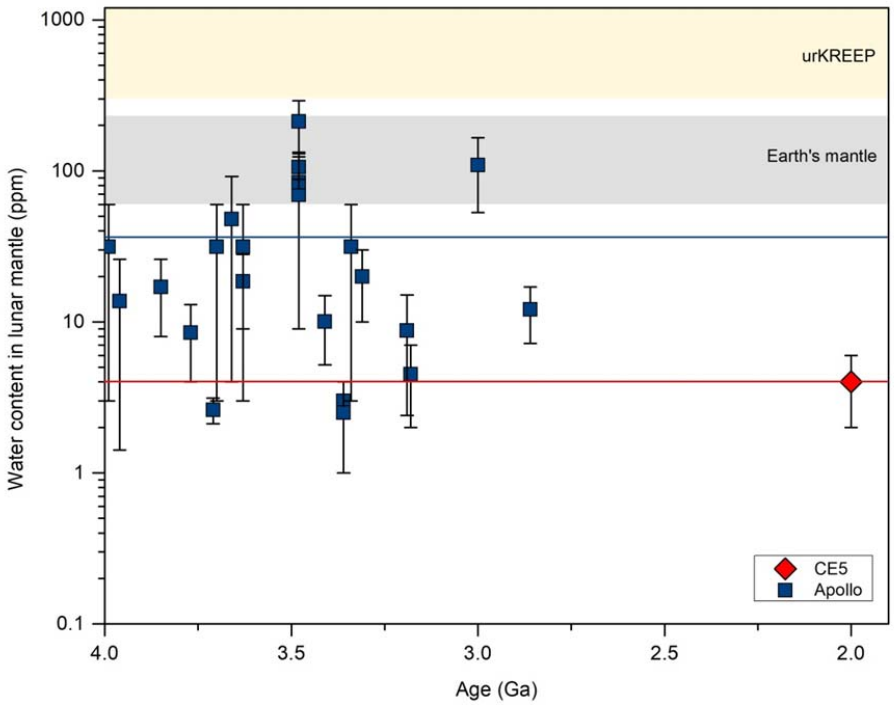

Fig. 3 | Variation of mantle water abundance estimates vs. crystallisation age of magmatic products. The maximum mantle water abundance at 2.03 Ga, which was estimated in this work using CE5 basalts, plots at the lower end of mantle water abundance estimates for Apollo and meteorites samples formed between ca. 4.0-2.8 Ga. All data are plotted as average values with the error bars representing the ranges of estimates. Estimates for the water abundances in urKREEP[25], the last dregs of the lunar magma ocean, and Earth's primitive mantle[40] are shown for comparison. Literature data are provided in Extended Data Table 5.

The water-rich melt inclusions have the lowest δD values (-330 ± 164‰), which is consistent with δD estimates for the lunar mantle made from analysis of various types of lunar samples[11, 16, 18-20, 22, 24]. This similarity suggests that the melt with the lowest δD was trapped in the early stages of magma crystallisation before substantial degassing of water in the form of H_2 (refs. [11, 15, 39]). On the other hand, the melt inclusions with higher δD (>270 ‰) also contain substantial water and overlap with the water-poor apatite (Fig. 3). This observation can be explained by the late crystallisation of ilmenite, when more water was concentrated in the residual melt before degassing loss and apatite became saturated in the melt.

As discussed above, the most deuterium-depleted melt inclusions likely captured the basaltic parent magma without notable degassing loss of water in the form of H_2. Hence, the highest water abundance (~370 $\mu g.g^{-1}$; Extended Data Table 3) of these melt inclusions can be referred to as the maximum water content of the basaltic magma, because a fraction of the constituent minerals could have precipitated before the earliest crystallised ilmenite. With further consideration of partial post-entrapped crystallisation of nominally anhydrous minerals (Fig. 2), which enhanced the water abundance of the glassy domain analyzed by the ion probe, the maximum water abundance of the parent magma of CE5 basalts could be to some extent lower than ~370 $\mu g.g^{-1}$. On the other hand, the water abundance of the parent magma can also be

estimated from a water content of ~8 $\mu g.g^{-1}$ for the bulk CE5 basalts through calibration for degassing loss of 98-99% water in the form of H_2 based on the accompanying δD increasing from ~-300‰ to the average of 578 ± 208‰ (1σ) (Extended Data Table 2, details see Supporting Information). This yields an estimate for the water abundance of the parent magma of 380-760 $\mu g.g^{-1}$, consistent with the highest melt inclusion water abundance. We thus use the highest melt inclusion water abundance (367 ± 29 $\mu g.g^{-1}$; Extended Data Table 3) as the maximum water abundance estimate for the parent basaltic magma.

The parent magma of CE5 basalts were derived from a depleted lunar mantle source not associated with a KREEP-component, based on its low initial μ value (680 ± 20) ($^{238}U/^{204}Pb$)[3], low initial $^{87}Sr/^{76}Sr$ ratio (0.69934 to 0.69986) and high positive $\varepsilon_{Nd}(t)$ (7.9 to 9.3)[4]. The elevated abundances of REE and Th, and high FeO and moderate TiO_2 concentrations of CE5 basalts match a model of low degrees (2-3%) of partial melting followed by 43-78% fractional crystallisation[4]. Accordingly, the maximum water concentration in the lunar mantle source beneath the Chang'E-5 landing site can be estimated at 2-6 $\mu g.g^{-1}$, corresponding to a maximum water abundance of ~370 $\mu g.g^{-1}$ in the derived basaltic magma (See Supporting Information).

In general, our analyses of apatite and melt inclusions outline the evolution of CE5 basalts, which can be divided into three stages. In Stage 1, the mantle source region underneath the PKT region with ~2-6 $\mu g.g^{-1}$ water experienced a low degree (2-3%) of partial melting followed by a moderate-to-high degree (43-78%) of fractional crystallisation[4], generating a basaltic magma with ~370 $\mu g.g^{-1}$ water and a δD of ~-300‰. This maximum water abundance, yielding our best estimate for the hydrogen isotopic composition of water in the parent magma, was recorded in the melt inclusions captured by the earliest-formed ilmenite analysed here. In Stage 2, H_2 degassing from the parent magma occurred during its ascent to shallower depths and on the surface of the Moon, and was accompanied by the crystallisation of ilmenite that entrapped melts at various stages of evolution. Extensive H_2 degassing[15,40] could have occurred in the reduced lunar environment[41, 42], resulting in extreme D/H fractionation from ~-300‰ up to ~300‰. In Stage 3, apatite crystallised from the residual melts that became enriched in water, halogens, and other incompatible species, after most nominally anhydrous silicates and ilmenite had formed.

The maximum water abundance of 2-6 $\mu g.g^{-1}$ estimated for the mantle source of CE5 basalts appears at the lower end of the mantle water abundance estimates derived from Apollo basalts and lunar meteorites[9-11, 15, 25] (Fig. 3). This could have important implications for understanding late volcanism on the Moon. First, such a dry mantle source for CE5 basalts excludes the possibility that a high abundance of water in the lunar mantle reservoir could be one of the main causes for the prolonged volcanic activity in this part of the PKT. Second, our observations indicate that the water abundance in the Moon's interior may have to some extent decreased from 4.0-2.8 Ga to 2.0 Ga (Fig. 3). This systematic loss of water over time could be a result of prolonged magmatic activity in the PKT, probably through multiple water-bearing melt extractions episodes from the PKT mantle reservoir during extended volcanic activity. In the northwestern PKT region, in close proximity to the CE5 landing site, up to 10 basaltic units ranging in age from 3.7 to 1.2 Ga have been identified[43], although it is difficult to be certain that all these units were derived from the same mantle source region. Nevertheless, such a dehydration partial melting process has also been observed in the Earth's mantle[44, 45].

Alternatively, the wide range of estimates for the water abundance in the mantle source regions of all studied lunar basaltic products may reflect a heterogeneous distribution of water in the Moon's interior, and/or possible contamination of some volcanic products by KREEP-components during either magma transport or in their mantle source regions during convective overturn of the lunar magma ocean[46, 47]. However, CE5 basalts have not been contaminated by KREEP-components, and were derived from a depleted mantle source[4]. Our estimate of the mantle water abundance based on CE5 basalts in the PKT region is thus a surprising and critical regional constraint on the distribution of water in the Moon's interior.

The parent magma of CE5 basalts contained ~370 $\mu g.g^{-1}$ water, which is roughly comparable to but on the lower side of estimates for Apollo basalts that crystallised from ca. 4 to 2.8 Ga[11, 15, 25]. Combining such water abundances with petrological evidence for low degrees of partial melting suggest that the mantle source region of CE5 was relatively depleted in water compared to the source regions of Apollo mare basalts. Additionally, the mantle source of CE5 basalts is also depleted in the heat-producing elements U, Th, and K, relative to the bulk silicate Moon[4]. Therefore, it remains an enigma to explain how mare basaltic volcanism was sustained as late as 2.0 Ga on the cooling Moon as the lunar interior should have been relatively cold by then.

Online content

Any methods, additional references, Nature Research reporting summaries, source data, extended data, supplementary information, acknowledgements, peer review information; details of author contributions and competing interests; and statements of data and code availability are available at online version of the paper.

References

1. Canup, R.M. and E. Asphaug Origin of the Moon in a giant impact near the end of the Earth's formation. *Nature* **412**,708-12 (2001).
2. Shearer, C.K., et al. Thermal and magmatic evolution of the moon. *Rev Mineral Geochem* **60**,365-518 (2006).
3. Li, Q.-L., et al. Timing of the latest volcanism on the Moon from Chang'E-5 basalts. *Submitted to Nature* (2021).
4. Tian, H.-C., et al. A non-KREEP origin for the Chang'E-5 basalts in the Procellarum KREEP Terrane. *Submited to Nature* (2021).
5. Borg, L.E., et al. Prolonged KREEP magmatism on the Moon indicated by the youngest dated lunar igneous rock. *Nature* **432**,209-11 (2004).
6. Compston, W., et al. The age of the Fra Mauro Formation: A radiometric older limit. *Earth Planet Sc Lett* **12**,55-58 (1971).
7. Lin, Y., et al. Evidence for an early wet Moon from experimental crystallization of the lunar magma ocean. **10**,14 (2017).
8. Hauri, E.H., et al. High pre-eruptive water contents preserved in lunar melt inclusions. *Science* **333**,213-5 (2011).
9. Chen, Y., et al. Water, fluorine, and sulfur concentrations in the lunar mantle. *Earth Planet Sc Lett* **427**,37-46 (2015).
10. Ni, P., et al. A melt inclusion study on volatile abundances in the lunar mantle. *Geochim Cosmochim Ac* **249**,17-41 (2019).
11. Stephant, A., et al. The hydrogen isotopic composition of lunar melt inclusions: An interplay of complex magmatic and secondary processes. *Geochim Cosmochim Ac* **284**,196-221 (2020).
12. Stephant, A., et al. The chlorine isotopic composition of the Moon: Insights from melt inclusions. *Earth Planet Sc Lett* **523**,115715 (2019).

13. Boyce, J.W., et al. Lunar apatite with terrestrial volatile abundances. *Nature* **466**,466-9 (2010).
14. McCubbin, F.M., et al. Nominally hydrous magmatism on the Moon. *Proc Natl Acad Sci U S A* **107**,11223-8 (2010).
15. Tartese, R., et al. The abundance, distribution, and isotopic composition of Hydrogen in the Moon as revealed by basaltic lunar samples: Implications for the volatile inventory of the Moon. *Geochim Cosmochim Ac* **122**,58-74 (2013).
16. Tartese, R., et al. Apatites in lunar KREEP basalts: The missing link to understanding the H isotope systematics of the Moon. *Geology* **42**,363-366 (2014).
17. Barnes, J.J., et al. Multiple reservoirs of volatiles in the Moon revealed by the isotopic composition of chlorine in lunar basalts. *Geochim Cosmochim Ac* **266**,144-162 (2019).
18. Barnes, J.J., et al. An asteroidal origin for water in the Moon. *Nature communications* **7**,11684 (2016).
19. Barnes, J.J., et al. The origin of water in the primitive Moon as revealed by the lunar highlands samples. *Earth Planet Sc Lett* **390**,244-252 (2014).
20. Barnes, J.J., et al. Early degassing of lunar urKREEP by crust-breaching impact(s). *Earth Planet Sc Lett* **447**,84-94 (2016).
21. Saal, A.E., et al. Hydrogen isotopes in lunar volcanic glasses and melt inclusions reveal a carbonaceous chondrite heritage. *Science* **340**,1317-20 (2013).
22. Hauri, E.H., et al. Water in the Moon's interior: Truth and consequences. *Earth Planet Sc Lett* **409**,252-264 (2015).
23. Hui, H.J., et al. Water in lunar anorthosites and evidence for a wet early Moon. *Nat Geosci* **6**,177-180 (2013).
24. Hui, H.J., et al. A heterogeneous lunar interior for hydrogen isotopes as revealed by the lunar highlands samples. *Earth Planet Sc Lett* **473**,14-23 (2017).
25. McCubbin, F.M., et al. Magmatic volatiles (H, C, N, F, S, Cl) in the lunar mantle, crust, and regolith: Abundances, distributions, processes, and reservoirs. *Am Mineral* **100**,1668-1707 (2015).
26. Hauri, E.H., et al. Origin and Evolution of Water in the Moon's Interior. *Annu Rev Earth Pl Sc* **45**,89-111 (2017).
27. Liu, Y., et al. Direct measurement of hydroxyl in the lunar regolith and the origin of lunar surface water. *Nat Geosci* **5**,779-782 (2012).
28. Treiman, A.H., et al. D-poor hydrogen in lunar mare basalts assimilated from lunar regolith. *Am Mineral* **101**,1596-1603 (2016).
29. Greenwood, J.P., et al. Hydrogen isotope ratios in lunar rocks indicate delivery of cometary water to the Moon. *Nat Geosci* **4**,79-82 (2011).
30. Qian, Y.Q., et al. Young lunar mare basalts in the Chang'e-5 sample return region, northern Oceanus Procellarum. *Earth Planet Sc Lett* **555**,116702 (2021).
31. Qian, Y.Q., et al. China's Chang'e-5 landing site: Geology, stratigraphy, and provenance of materials. *Earth Planet Sc Lett* **561**,116855 (2021).
32. Boyce, J.W., et al. The chlorine isotope fingerprint of the lunar magma ocean. *Sci Adv* **1**,e1500380 (2015).
33. Barnes, J.J., et al. Accurate and precise measurements of the D/H ratio and hydroxyl content in lunar apatites using NanoSIMS. *Chem Geol* **337**,48-55 (2013).
34. Pernet-Fisher, J.F., et al. Estimating the lunar mantle water budget from phosphates: Complications associated with silicate-liquid-immiscibility. *Geochim Cosmochim Ac* **144**,326-341 (2014).
35. Singer, J.A., et al. Evidence for the solar wind in lunar magmas: A study of slowly cooled samples of the Apollo 12 olivine basalt suite. *Geochem J* **51**,95-104 (2017).
36. Robinson, K.L. and G.J. Taylor Heterogeneous distribution of water in the Moon. *Nat Geosci* **7**,401-408 (2014).
37. Curran, N.M., et al. A database of noble gases in lunar samples in preparation for mass spectrometry on the Moon. *Planet Space Sci* **182**,104823 (2020).
38. Horz, F., et al., *Lunar surface processes*, in *Lunar Sourcebook, a user's guide to the Moon*. 1974. p. 61-120.
39. Sharp, Z.D., F.M. McCubbin, and C.K. Shearer A hydrogen-based oxidation mechanism relevant to planetary formation. *Earth Planet Sc Lett* **380**,88-97 (2013).
40. Saal, A.E., et al. Vapour undersaturation in primitive mid-ocean-ridge basalt and the volatile content of Earth's upper mantle. *Nature* **419**,451-5 (2002).

41. Ustunisik, G., H. Nekvasil, and D. Lindsley Differential degassing of H2O, Cl, F, and S: Potential effects on lunar apatite. *Am Mineral* **96**,1650-1653 (2011).
42. Ustunisik, G., et al. Degassing pathways of Cl-, F-, H-, and S-bearing magmas near the lunar surface: Implications for the composition and Cl isotopic values of lunar apatite. *Am Mineral* **100**,1717-1727 (2015).
43. Qian, Y.Q., et al. Geology and Scientific Significance of the Rümker Region in Northern Oceanus Procellarum: China's Chang'E‐5 Landing Region. *J Geophys Res-Planet* **123**,1407-1430 (2018).
44. Ardia, P., et al. H2O storage capacity of olivine at 5–8GPa and consequences for dehydration partial melting of the upper mantle. *Earth Planet Sc Lett* **345-348**,104-116 (2012).
45. Asimow, P.D. and C.H. Langmuir The importance of water to oceanic mantle melting regimes. *Nature* **421**,815-20 (2003).
46. Ringwood, A. and S. Kesson A dynamic model for mare basalt petrogenesis. Lunar and Planetary Science Conference Proceedings **7**,1697-1722 (1976).
47. Hess, P.C. and E.M. Parmentier A model for the thermal and chemical evolution of the Moon's interior: implications for the onset of mare volcanism. *Earth Planet Sc Lett* **134**,501-514 (1995).

Methods

Sample preparation

Two Chang'E-5 (CE5) lunar soils (CE5C0100YJFM00103, ~1g, CE5C0400YJFM00406, ~2g) allocated by the China National Space Administration were used in this study. Both of them were scooped by the robotic arm of the CE5 lander and separated into different packages in the ultraclean room at the extraterrestrial sample curation center of the National Astronomical Observatories, Chinese Academy of Sciences. Approximately 240 soil fragments with grain sizes varying from ~100 μm to ~ 1 mm were sieved and hand-picked under a binocular microscope in the ultraclean room at the Institute of Geology and Geophysics, Chinese Academy of Sciences (IGGCAS). Then, about 2/3 of the picked grains were prepared as 8 Sn-Bi metal-alloy mounts following the method of Zhang et al. (2018)[48] and the other 1/3 was mounted in epoxy and prepared as 3 polished thin sections. The polished metal mounts and thin sections were cleaned using ultrapure water and anhydrous ethanol prior to drying at 70 ℃ in a baking oven overnight. The details of apatite and ilmenite-hosted melt inclusions from 23 CE5 basalt clasts and fragments are summarised in Extended Data Table 1.

Scanning Electron Microscope (SEM) observation

Petrographic observations and elemental mapping were carried out using field emission scanning electron microscopes (FE-SEM) using FEI Nova NanoSEM 450 and Thermofisher Apreo instruments at the IGGCAS, using electron beam currents of 2 to 3.2 nA and an acceleration voltage of 15 kV. Energy dispersive spectroscopy (EDS) X-ray maps were collected for each basaltic clasts to quickly locate P-bearing phases. The phosphates were then observed at higher magnification in back-scattered electron (BSE) images. The modal abundance of apatite from various CE5 basalt clasts were counted by the exposed surface areas (Table S1). The prepared sections were initially coated with Au to identify apatite and melt inclusions for *in situ* NanoSIMS measurement of water content and hydrogen isotopes. Another round of SEM observation was carried out after NanoSIMS measurement to confirm the positions of the NanoSIMS spots.

Electron probe microanalysis

We used a JEOL JXA-8100 electron probe micro-analyzer (EPMA) at the IGGCAS to quantify the major and minor elemental abundances in phosphates, melt inclusions in ilmenite, and associated mafic minerals (i.e. clinopyroxene, olivine, plagioclase, and ilmenite). The samples were coated with carbon. The operating accelerating voltage was 15 kV and the beam current was 20 nA. The EPMA analyses were carried out after the NanoSIMS measurements in order to avoid possible H loss due to bombardment by the electron beam[33]. The EPMA standards were natural albite (Na and Al), bustamite (Mn), diopside (Ca, Si, and Mg), apatite (P), K-feldspar (K), tugtupite (Cl), synthetic fluorite (F), rutile (Ti), Fe_2O_3 (Fe), V_2O_5 (V), NiO (Ni), and Cr_2O_3 (Cr). Sodium, K, F, and Cl were first measured in order to minimise possible loss of volatiles by electron beam irradiation. The detection limits were (1σ) 0.01 wt% for Cl and S, 0.02 wt% for Na, Mg, Al, Cr, K, Si, Mn, Ca and Fe, 0.03 wt% for F, Ba, Ni and Ti, 0.04 wt% for P. A program based on the ZAF procedure was used for data correction. The EPMA data obtained for apatite, melt inclusions in ilmenite, and the coexisting silicates are listed in Table S2.

In situ water abundance and hydrogen isotope analysis

Apatite and melt inclusions

The hydrogen isotopes and water content of apatite and melt inclusions enclosed in ilmenite from the CE5 basaltic clasts were measured with a CAMECA NanoSIMS 50L at IGGCAS. The samples were coated with Au, were loaded in sample holders together with the standards, and were baked overnight at ~60 ºC in the NanoSIMS airlock. The holders were then stored in the NanoSIMS sample chamber to improve the vacuum quality and minimise the H background[49-51]. The vacuum pressure in the analysis chamber was 2.8×10^{-10} to 3.0×10^{-10} mbar during analysis. Each 15 μm × 15 μm analysis area was pre-sputtered for ~ 2 mins with a Cs^+ ion beam current of ~ 2 nA to remove the surface coating and potential contamination. During analysis, the secondary anions $^1H^-$, $^2D^-$, $^{12}C^-$, and $^{16}O^-$ were simultaneously counted by electron multipliers (EMs) and a Faraday cup from the central 3 μm × 3 μm areas using the NanoSIMS blanking technique. A 44 ns dead time was corrected for all EMs, while the EM noise ($<10^{-2}$ cps) was ignored. We used a primary ion beam current of ~0.5 nA for analysis, corresponding to a beam size of ~500 nm in diameter. The charging effect on the samples surface was compensated by an electron-gun during analysis. A chip of the anhydrous San Carlos olivine was used for H background corrections, following the relationship: $H/O_{bg} = (H_{counts} - H_{bg}) / O_{counts}$ and $D/H_{measured} = (1-f) \times D/H_{true} + f \times D/H_{bg}$, where f is the proportion of H emitted from the instrumental background[52]. Here, D/H_{bg} was 3.36 (±0.55)$\times10^{-4}$ and H_{bg} = 7.36 (±1.49) × 10^4 (2SD, N=11, corresponding to H_2O background abundance of 25 ± 8 μg.g^{-1} (2SD)). Corrections for matrix effects and instrumental mass fractionation (IMF) on water abundance (Extended Data Fig. 2) and H isotope determination (Extended Data Fig. 3) were determined by measuring two apatite standards, Durango apatite (H_2O = 0.0478 wt% and δD = -120 ± 5‰) [29, 53] and Kovdor apatite (H_2O = 0.98 ± 0.07 wt.% and δD = -66 ± 21‰)[54], the SWIFT MORB glass (H_2O = 0.258 wt.% and δD = -73 ± 2‰), and two basaltic glasses, 519-4-1 (H_2O = 0.17 wt.%)[49] and 1833-11 (H_2O = 1.2 wt.%)[49] (Table S3). Hydrogen isotopic compositions are given using the delta notation, δD = $((D/H)_{sample}/(D/H)_{SMOW})$-1) ×1000 ‰, where SMOW is the standard mean ocean water with a D/H ratio of 1.5576×10^{-4}. More technical details can be found in to Hu et al. (2014, 2015)[50, 51]. All data are reported with their 2σ uncertainties that include reproducibility of D/H measurements on the reference materials, uncertainty of H_2O background subtraction, and internal precision on each analysis (Extended Data Tables 2 and 3 and Table S4). The raw measured D/H ratios were corrected for the background, followed by correction for IMF.

Clinopyroxene

The water abundance of clinopyroxene from the CE5 basaltic clasts was measured with the CAMECA NanoSIMS 50L using an identical instrument setup to that described above. We used a higher Cs^+ primary beam current of 7 nA to improve the $^1H^-$ counts on clinopyroxene. Each 25 μm × 25 μm analysis areas was pre-sputtered for ~ 2 mins with the same analytical beam current to remove surface coating and potential contaminations. The secondary ion signals from the central 7 μm × 7 μm areas were counted with 50% blanking of outermost regions. San Carlos olivine (H_2O = 1.4 μg.g^{-1}, ref. [55]) was used for determining instrumental background of H. The analytical results are listed in Extended Data Table 4.

Correction of water abundances and D/H ratios for spallation effects

The measured D/H ratios have also been corrected for the potential effects of spallation by cosmic-ray, using a D production rate of 2.17×10^{-12} mol D/g/Ma[56] for melt inclusions and 9.20×10^{-13} mol D/g/Ma[57] for apatite. The correction errors induced by D spallation are around 50% on δD and negligible on water content[21]. The cosmic ray exposure (CRE) ages determined for

most Apollo samples are less than ~200 Ma[37]. Because no CRE age is yet available for the Chang'E-5 basaltic clasts, we modeled the effects of corrections for CRE ages of 10, 50, 100 and 200 Ma (Extended Data Table 3 and Fig. 4). The corrected δD values for the melt inclusions with low water abundances appear to be over-corrected for CRE ages of 100 and 200 Ma, as indicated by unusually low δD values. We thus decided to correct δD values using a CRE age of 50 Ma, slightly older than that of Apollo lithic fragments (1-24 Ma) [58], for which the corrected δD values of the melt inclusions with low H_2O are comparable to the lowest δD values measured in apatite (~300‰), as apatite crystallization postdated that of ilmenite in which the melt inclusions are hosted.

Degassing modeling

The hydrogen isotope fractionation during volatile loss into a vacuum is given by $\alpha^2 = M1/M2$, where M1 and M2 are the masses of the volatile phase isotopologues. The change of the isotopic composition of H during volatile loss by Rayleigh fractionation is given by $R = R_0 \times f^{(\alpha-1)}$, where R_0 and R are the initial and final D/H ratios for a fraction *f* of remaining hydrogen[39]. Degassing of H_2 (M1 = 2 for H_2 and M2 = 3 for HD) yields an α value of ~0.8165, and degassing of H_2O (M1 = 18 for H_2O and M2 = 19 for HDO) yields an α value of ~0.9733[39] (Extended Data Fig. 4).

References

48. Zhang, W.F., et al. A novel sample preparation method for ultra-high vacuum (UHV) secondary ion mass spectrometry (SIMS) analysis. *J Anal Atom Spectrom* **33**,1559-1563 (2018).
49. Hauri, E., et al. SIMS analysis of volatiles in silicate glasses 1. Calibration, matrix effects and comparisons with FTIR. *Chem Geol* **183**,99-114 (2002).
50. Hu, S., et al. NanoSIMS analyses of apatite and melt inclusions in the GRV 020090 Martian meteorite: Hydrogen isotope evidence for recent past underground hydrothermal activity on Mars. *Geochim Cosmochim Ac* **140**,321-333 (2014).
51. Hu, S., et al. Measurements of water content and D/H ratio in apatite and silicate glasses using a NanoSIMS 50L. *J Anal Atom Spectrom* **30**,967-978 (2015).
52. Tartese, R., M. Anand, and I.A. Franchi H and Cl isotope characteristics of indigenous and late hydrothermal fluids on the differentiated asteroidal parent body of Grave Nunataks 06128. *Geochim Cosmochim Ac* **266**,529-543 (2019).
53. Greenwood, J.P., et al. Hydrogen isotope evidence for loss of water from Mars through time. *Geophys Res Lett* **35**,L05203 (2008).
54. Nadeau, S.L., S. Epstein, and E. Stolper Hydrogen and carbon abundances and isotopic ratios in apatite from alkaline intrusive complexes, with a focus on carbonatites. *Geochim Cosmochim Ac* **63**,1837-1851 (1999).
55. Zhang, W.F., et al. Optimization of SIMS analytical parameters for water content measurement of olivine. *Surf Interf Anal* **52**,224-233 (2019).
56. Furi, E., E. Deloule, and R. Trappitsch The production rate of cosmogenic deuterium at the Moon's surface. *Earth Planet Sc Lett* **474**,76-82 (2017).
57. Merlivat, L., et al., *Spallation deuterium in rock 70215*, in *Lunar and Planetary Science Conference Proceedings*. 1976. p. 649-658.
58. Das, J.P., S.L. Baldwin, and J.W. Delano 40Ar/39Ar and cosmic ray exposure ages of plagioclase-rich lithic fragments from Apollo 17 regolith, 78461. *Earth Planet Space* **68**,11 (2016).
59. Guggisberg, S., et al. Classification of the Apollo-11 mare basalts according to/Ar-39/-/Ar-40/ages and petrological properties. Lunar and Planetary Science Conference Proceedings **10**,1-39 (1979).
60. Papanastassiou, D., G. Wasserburg, and D. Burnett Rb-Sr ages of lunar rocks from the Sea of Tranquillity. *Earth Planet Sc Lett* **8**,1-19 (1970).
61. Nyquist, L., et al. The SR and Nd isotopic record of Apollo 12 basalts-Implications for lunar geochemical evolution. Lunar and Planetary Science Conference Proceedings **10**,77-114 (1979).

62. Papanastassiou, D. and G. Wasserburg RbSr ages of igneous rocks from the Apollo 14 mission and the age of the Fra Mauro formation. *Earth Planet Sc Lett* **12**,36-48 (1971).
63. Saal, A.E., et al. Volatile content of lunar volcanic glasses and the presence of water in the Moon's interior. *Nature* **454**,192-5 (2008).
64. Snyder, G., et al. Volcanism in the Hadley-Apennine region of the Moon: Geochronology, Nd-Sr isotopic systematics, and depths of melting. Lunar and Planetary Science Conference 1141 (1998).
65. Husain, L. 40Ar-39Ar chronology and cosmic ray exposure ages of the Apollo 15 samples. *Journal of Geophysical Research* **79**,2588-2606 (1974).
66. Tatsumoto, M., W.R. Premo, and D.M. Unruh Origin of Lead from Green Glass of Apollo-15426 - a Search for Primitive Lunar Lead. *J Geophys Res-Solid* **92**,E361-E371 (1987).
67. York, D., W.J. Kenyon, and R.J. Doyle 40Ar-39Ar ages of Apollo 14 and 15 samples. Lunar and Planetary Science Conference Proceedings **3**,1613 (1972).
68. Saito, K. and E. Alexander 40AR-39AR Studies of Lunar Soil 74001. Lunar and Planetary Science Conference **10**,1049-1051 (1979).
69. Furi, E., et al. New evidence for chondritic lunar water from combined D/H and noble gas analyses of single Apollo 17 volcanic glasses. *Icarus* **229**,109-120 (2014).
70. Tera, F. and G. Wasserburg Lunar ball games and other sports. Lunar and Planetary Science Conference **7**,(1976).
71. Tera, F., D.A. Papanastassiou, and G.J. Wasserburg Isotopic Evidence for a Terminal Lunar Cataclysm. *Earth Planet Sc Lett* **22**,1-21 (1974).
72. Fernandes, V.A., R. Burgess, and A. Morris 40Ar‐39Ar age determinations of lunar basalt meteorites Asuka 881757, Yamato 793169, Miller Range 05035, La Paz Icefield 02205, Northwest Africa 479, and basaltic breccia Elephant Moraine 96008. *Meteorit Planet Sci* **44**,805-821 (2009).
73. Anand, M., et al. Petrology and geochemistry of LaPaz Icefield 02205: A new unique low-Ti mare-basalt meteorite. *Geochim Cosmochim Ac* **70**,246-264 (2006).
74. Yang, W. and Y. Lin New lunar samples returned by Chang'E-5: Opportunities for new discoveries and international collaboration. *The Innovation* **2**,100070 (2021).

Data availablility

All geochemical data generated in this study are included in Extended Data Table 1-4 and in Supplementary Table S1-S5.

Code availability

No code is used in this study.

Acknowledgements

We thank David Chew for providing Durango and Kovdor apatite, Erik Hauri for providing basaltic glass 519-4-1 and 1833-11, Robert Francis for providing SWIFT MORB glass, Ross Mitchell, Xian-Hua Li, and Fu-Yuan Wu for constructive comments, Yi Chen and Lihui Jia for the assistance on EPMA measurement, Hongxia Ma and Danping Zhang for hand picking the CE5 soil fragments, and Jiangyan Yuan and Xu Tang for the assistance on SEM observation. This study was funded by the Strategic Priority Research Program of Chinese Academy of Sciences (XDB 41000000), the key research program of Chinese Academy of Sciences (ZDBS-SSW-JSC007-15), and the key research program of the Institute of Geology and Geophysics, Chinese Academy of Sciences (IGGCAS-202101 and 201904), the National Natural Science Foundation of China (41973062), and Pre-research project on Civil Aerospace Technologies by CNSA (D020201 and D020203). MA and RT acknowledge funding from the UK Science and Technology Facilities Council (grant #ST/P000657/1 and # ST/P005225/1, resp.). The CE5 samples were allocated by the China National Space Administration.

Author contributions

S. H., Y. L., and H. H. designed this research. J. J., H. H., Y. Y., J. L., L. G., Q. G., and S. H. prepared the sample and characterized the petrography and mineral chemistry of CE5 basalts. H. H., J. H., R. L., J. J., and S. H conducted the NanoSIMS measurements. S. H., Y. L., H.H., J. J., H. H, M. A., R. T., and H. H. wrote the manuscript. All authors contributed to the preparation of the manuscript.

Competing interests: The authors declare no competing interests.

Additional information

Extended Data Table 1 | The Chang'E-5 basalt clasts

Clast No.	Mount form*	Size (mm)	Texture	Apatite (μm)	Melt inclusion (μm)
CE5C0100YJFM00406					
406-010,001	Sn-Bi alloy	0.87×0.39	Poikilitic	~3	
406-010,019	Sn-Bi alloy	0.58×0.35	Poikilitic	~3	
406-010,023	Sn-Bi alloy	0.79×0.57	Poikilitic	10	17×11
406-011,003	Sn-Bi alloy	0.89×0.59	Equigranular	5 to 10	
406-011,007	Sn-Bi alloy	0.70×0.30	Poikilitic	3 to 5	
406-012,004	Sn-Bi alloy	0.89×0.58	Subophitic	3 to 5	
406-012,009	Sn-Bi alloy	0.69×0.611	Fragment	~3	<50×17
406-014,001	PTS	0.39×0.18	Fragment	<10	
406-014,003	PTS	0.80×0.71	Subophitic	~5	
406-015,001	PTS	1.17×0.72	Fragment	10	
406-015,014	PTS	0.25×0.15	Equigranular	10	
406-015,045	PTS	0.51×0.39	Subophitic	3 to 5	19×7
406-015,046	PTS	0.67×0.29	Subophitic	3 to 5	6×4
406-015,048	PTS	0.59×0.36	Subophitic	5 to 10	
406-015,059	PTS	0.68×0.30	Poikilitic	3 to 5	
CE5C0100YJFM00103					
103-017,001	Sn-Bi alloy	1.05×0.42	Poikilitic	~3	55×40
103-017,010	Sn-Bi alloy	0.45×0.27	Equigranular	~5	
103-017,011	Sn-Bi alloy	0.64×0.44	Equigranular	~5	
103-015,013	Sn-Bi alloy	0.54×0.52	Poikilitic	~5	10×7
103-020,004	PTS	0.25×0.24	Fragment	10	
103-020,013	PTS	0.37×0.21	Fragment		25×13
103-020,018	PTS	0.41×0.30	Fragment	<3	17×4
103-020,021	PTS	0.39×0.23	Poikilitic	5 to 10	

*Sn-Bi alloy mount, PTS-polished thin section.

Extended Data Table 2 | Water abundance and hydrogen isotopes of CE5 apatite

		CRE age = 0 Ma				CRE age = 50 Ma*	
File Name	Clast No.	H_2O μg.g^{-1}	2σ μg.g^{-1}	δD ‰	2 σ ‰	H_2O μg.g^{-1}	δD ‰
010-001Ap-1	406-010,001	2205	91	382	64	2205	381
010-001Ap-2	406-010,001	1850	79	461	67	1850	460
010-019Ap-1	406-010,019	2418	109	422	65	2418	421
010-019Ap-2	406-010,019	2153	96	363	64	2153	362
010-023Ap-1	406-010,023	176	17	722	169	176	708
010-023Ap-2	406-010,023	236	19	426	159	235	416
010-023Ap-3	406-010,023	110	13	440	210	110	418
011-003Ap-1	406-011,003	2936	119	464	62	2936	463
011-007Ap-1	406-011,007	1626	73	276	69	1626	275
012-004Ap-1	406-012,004	2595	108	382	70	2595	381
012-004Ap-2	406-012,004	2755	110	456	60	2755	455
012-009Ap-1	406-012,009	1936	87	551	67	1936	550
014-001Ap-1	406-014,001	4363	187	329	57	4363	329
014-001Ap-2	406-014,001	1841	82	368	67	1841	367
014-003Ap-1	406-014,003	4856	217	376	66	4856	376
015-001Ap-1	406-015,001	1137	53	368	80	1137	366
015-001Ap-2	406-015,001	1167	56	512	80	1166	510
015-001Ap-3	406-015,001	939	46	566	84	939	563
015-014Ap-1	406-015,014	1717	74	931	63	1717	929
015-014Ap-2	406-015,014	1652	71	814	64	1651	812
015-014Ap-3	406-015,014	791	40	723	83	791	720
015-014Ap-4	406-015,014	1461	64	834	69	1461	832
015-014Ap-5	406-015,014	1983	88	857	61	1983	856
015-014Ap-6	406-015,014	1214	54	878	70	1213	877
015-014Ap-7	406-015,014	1139	52	861	70	1138	859
015-014Ap-8	406-015,014	1312	59	1024	71	1312	1022
015-014Ap-9	406-015,014	1217	54	826	70	1217	824
015-014Ap-10	406-015,014	1516	67	886	65	1516	884
015-014Ap-11	406-015,014	2361	98	930	59	2361	929
015-014Ap-12	406-015,014	952	45	703	78	952	700
015-046Ap-1	406-015,046	1574	69	368	75	1574	367
015-048Ap-1	406-015,048	1127	65	609	77	1127	607
015-059Ap-1	406-015,059	1166	57	754	77	1166	752
017-010Ap-1	103-017,010	1606	75	321	73	1606	320
017-011Ap-1	103-017,011	1714	80	412	68	1714	411
017-011Ap-2	103-017,011	2322	96	479	65	2322	478
017-013Ap-1	103-017,013	1920	87	562	66	1920	561
020-018Ap-1	103-020,018	555	31	564	98	555	560
020-021Ap-1	103-020,021	3681	169	511	55	3681	511
020-021Ap-2	103-020,021	3077	134	563	58	3077	562
020-004Ap-1	103-020,004	1807	82	451	70	1807	450
020-004Ap-2	103-020,004	2164	91	519	64	2164	518
020-004Ap-3	103-020,004	2049	93	509	64	2049	508

*D production rate of 9.20 × 10^{-13} mol D/g/Ma[57] was used for cosmogenic spallation effects. CRE age: cosmic ray exposure age.

Extended Data Table 3 | Water abundance and hydrogen isotopes of CE5 ilmenite-hosted melt inclusions

		CRE age = 0 Ma				CRE age = 50 Ma*	
File Name	**Clast No.**	**H_2O μg.g^{-1}**	**2σ μg.g^{-1}**	**δD ‰**	**2σ ‰**	**H_2O μg.g^{-1}**	**δD ‰**
010-023MI-1	406-010,023	26	6	411	349	26	177
012-009MI-1	406-012,009	89	16	-147	322	89	-216
015-045MI-1	406-015,045	661	37	281	113	661	271
015-046MI-1	406-015,046	174	18	581	161	174	547
017-013MI-1	406-017,013	93	15	933	224	93	869
017-001MI-1	406-017,001	27	6	243	339	27	18
017-001MI-2	406-017,001	13	4	669	390	13	202
020-013MI-1	103-020,013	367	29	-313	164	367	-330
020-013MI-2	103-020,013	281	23	-310	182	281	-332
020-018MI-1	103-020,018	114	11	-180	213	114	-234
020-018MI-2	103-020,018	154	13	-94	180	154	-133

*D production rate of 2.17×10^{-12} mol D/g/Ma[56] was used for correction of comogenic spallation effects. CRE age: cosmic ray exposure age.

Extended Data Table 4 | H/O ratios of CE5 clinopyroxene and reference San Carlos olivine measured by NanoSIMS 50L

Clast No.	Grain#	$^{1}H_{Counts}$	$^{16}O_{Counts}$	$^{1}H/^{16}O$	Err Mean	Poisson
Standard	SanCarlosOl-1	1.39E+05	5.40482E+010	2.58E-06	8.500E-001	2.68E-01
Standard	SanCarlosOl-2	1.19E+05	4.64532E+010	2.56E-06	1.150E+000	2.90E-01
Standard	SanCarlosOl-3	1.12E+05	4.12918E+010	2.71E-06	8.360E-001	2.99E-01
Standard	SanCarlosOl-4	6.21E+04	4.62124E+010	1.34E-06	7.490E-001	4.01E-01
Avg.				*2.30E-6*		
406-016,017	016-017CPX-1	5.11E+04	4.94974E+010	1.03E-06	8.820E-001	4.42E-01
406-016,017	016-017CPX-2	5.78E+04	5.46378E+010	1.06E-06	8.260E-001	4.16E-01
406-012,009	012-009CPX-1	3.69E+04	6.13187E+010	6.02E-07	7.830E-001	5.20E-01
103-017,010	017-010CPX-1	5.07E+04	5.30020E+010	9.56E-07	1.170E+000	4.44E-01
406-010,023	010-023CPX-1	4.61E+04	6.48510E+010	7.11E-07	7.980E-001	4.66E-01
103-020,013	020-013CPX-1	6.37E+04	5.12381E+010	1.24E-06	7.200E-001	3.96E-01
406-016,013	020-013CPX-2	5.85E+04	5.46135E+010	1.07E-06	8.240E-001	4.13E-01
406-016,011	016-011CPX-1	7.20E+04	5.62715E+010	1.28E-06	5.990E-001	3.73E-01
103-018,001	018-001CPX-1	4.44E+04	5.91575E+010	7.50E-07	6.450E-001	4.75E-01
103-018,005	018-001CPX-2	4.74E+04	6.10594E+010	7.76E-07	5.610E-001	4.60E-01
406-016,005	016-005CPX-1	4.79E+04	7.38569E+010	6.49E-07	5.150E-001	4.57E-01
103-020,001	020-001CPX-1	7.99E+04	6.41275E+010	1.25E-06	4.660E-001	3.54E-01
103-020,018	020-018CPX-1	6.81E+04	6.03355E+010	1.13E-06	5.150E-001	3.83E-01
103-020,018	020-018CPX-2	6.58E+04	5.82048E+010	1.13E-06	8.080E-001	3.90E-01
406-010,023	010-023CPX-2	4.01E+04	6.86893E+010	5.84E-07	6.320E-001	4.99E-01
406-010,019	010-019CPX-1	4.60E+04	7.55480E+010	6.09E-07	6.740E-001	4.66E-01
406-010,019	010-019CPX-2	3.72E+04	6.61077E+010	5.62E-07	6.840E-001	5.19E-01
406-010,019	010-019CPX-3	3.72E+04	6.90618E+010	5.39E-07	7.200E-001	5.18E-01
Avg.				*8.85E-7*		

Extended Data Table 5 | Summary of the water abundances estimated for the lunar mantle source regions of basaltic products formed between ca. 4-2 Ga.

Sample name	Age (Ga)*	References	Phase#	H_2O_{min} (μg.g^{-1})	H_2O_{max} (μg.g^{-1})	References
10020	3.7	59	MI	3	60	11
10044	3.71	60	Ap	2.12	3.12	29, 33
10058	3.63	60	Ap	9	28	15
10058	3.63	60	MI	3	60	11
12002	3.36	60	MI	3	3	11
12004	3.36	60	MI	3	3	11
12008	3.36	60	MI	3	3	11
12018	ND		MI	25	160	11, 35
12020	3.36	60	MI	3	3	11
12039	3.19	61	Ap	2.4	15.12	15, 28, 29, 32
12040	3.36	60	MI	3	3	11
12064	3.18	62	Ap	2	7	25, 33
14053	3.96	62	Ap	1.42	26	29, 34, 63
14072	3.99	6	MI	3	60	11
15016	3.34	64	MI	3	60	11
15058	3.36	65	Ap	1	4	14, 15
15427	3.41	66	GB	5.2	14.9	63
15555	3.31	67	Ap	10	30	15
74002	3.66	68	GB	4	92	69
74220	3.48	70	MI	9	130	8, 25
74220	3.48	70	MI	133	292	22
74220	3.48	70	MI	88	124	9
74235	3.48	70	MI	84	84	10
75055	3.77	71	Ap	4	13	28, 29, 32
NWA 2977	2.86	5	Ap	7.2	17	14
MIL 05035	3.85	72	Ap	8	26	15
LAP 04841	3.0	73	Ap	53	166	15
CE5	2.03	3	MI	2	6	This study

*ND=No data.

#MI-Melt inclusions, Ap-Apatite, GB-Glass bead. They were used for estimating water abundance in the lunar mantle.

Supplementary Files

This is a list of supplementary files associated with this preprint. Click to download.

- SI.pdf
- Hu2021CE5H2OMethodsXextendeddataV9submitted.pdf